Analytical Methods

PAPER

View Article Online
View Journal | View Issue

Cite this: *Anal. Methods*, 2018, **10**, 2450

A visual detection of bisphenol A based on peroxidase-like activity of hemin–graphene composites and aptamer†

Zhengwei Xiong,‡[a] Haixia Zhong,‡[b] Shuang Zheng,[b] Pengxi Deng,[c] Ning Li,*[b] Wen Yun *[b] and Lizhu Yang*[c]

Received 27th March 2018
Accepted 2nd May 2018

DOI: 10.1039/c8ay00677f

rsc.li/methods

Herein, a fast and visible colorimetric method for bisphenol A (BPA) detection was developed using hemin-functionalized reduced graphene oxide (H–rGO) composites and aptamer. The aptamer can be stably adsorbed on the surface of H–rGO, preventing H–rGO from salt-induced aggregation. However, in the presence of BPA, the aptamer can bind with BPA; this results in the aggregation of H–rGO. Consequently, the supernatant contains a little H–rGO and shows light blue color after the chromogenic reaction. The color difference can be used for the quantitative detection of BPA. The designed aptasensor displayed a linear response for BPA in the range from 5 nM to 100 nM with a detection limit of 2 nM. This colorimetric aptasensing platform offered great advantages, including label-free conditions and visible result readout platform, for quick screening of BPA for on-site analysis and in-house diagnosis.

1. Introduction

Bisphenol A (BPA) is a significant organic chemical raw material. It is also an important derivative of phenol and acetone.[1,2] The addition of BPA (as a lining) to containers can prevent acidic vegetables and fruits from the internal erosion of the metal containers in which they are stored; therefore, it is widely used in canned food and beverage packaging, water bottles, and other hundreds of daily use plastic products.[3,4] Inhaling BPA powder is harmful to liver function and renal function; it may also reduce blood hemoglobin content in serious conditions.[5,6] Simultaneously, BPA shows hormone-like properties even at very low content (from 10^{-10} to 10^{-8} M). It can cause heart disease and affect the endocrine system; this has raised consumer concerns about the use of its products and food containers.[7,8] Therefore, convenient BPA detection methods with high sensitivity are of great importance for food safety and human health.

A number of BPA analytical methods have been established such as high performance liquid chromatography (HPLC),[9,10] gas chromatography (GC),[11] liquid chromatography coupled with mass spectrometry (LC-MS),[12,13] and gas chromatography coupled with mass spectrometry (GC-MS).[14,15] These traditional analytical technologies are highly sensitive with low detection limits. However, they are time-consuming and expensive and also need complex pre-processing procedures. In addition, complex instruments and skilled operators are required. Therefore, these technologies are not suitable for quick screening of BPA for on-site analysis and in-house diagnosis.

Aptamer is a single strand of oligonucleotides with high affinity and specificity for targets such as metal ions,[16,17] small molecules[18,19] and protein.[20,21] Aptamers have unique advantages such as desirable storage condition, easy chemical synthesis and biological compatibility.[22,23] The hemin-functionalized reduced graphene oxide (H–rGO) composites possess the advantages of these two materials.[24,25] Moreover, H–rGO shows different dispersions at high salt concentrations for single-stranded or double stranded DNA sequences.[26] In addition, the hemin on the surface of graphene can catalyze the reaction of peroxidase substrates with intrinsic peroxidase-like activity. Many kinds of typical nanomaterials, including Fe_3O_4,[27] AuNPs,[28] graphene oxide,[29] graphitic carbon nitride,[30] MoS_2,[31] WS_2,[32] MIL-53(Fe)[33] *etc.*, have peroxidase-like activity. Recently, H–rGO composites have been used for the detection of telomerase activity,[34] single nucleotide polymorphism[35] and DNA damage.[36] Therefore, H–rGO possesses wide application prospects as intrinsic peroxidase-like materials.[37]

In this study, a simple and label-free colorimetric method for BPA detection based on H–rGO and aptamer was developed.

[a]*School of Biological and Chemical Engineering, Chongqing University of Education, Chongqing, 400067, China*

[b]*Chongqing Key Laboratory of Catalysis and New Environmental Materials, College of Environment and Resources, Chongqing Technology and Business University, Chongqing, 400067, China. E-mail: 157020769@qq.com; 44863542@qq.com; Fax: +86-023-62768056; Tel: +86-023-62768056*

[c]*School of Pharmaceutical Sciences, Wenzhou Medical University, Wenzhou, Zhejiang, 325035, China. E-mail: yanglz3000@aliyun.com; Fax: +86-577-86689981; Tel: +86-577-86689984*

† Electronic supplementary information (ESI) available. See DOI: 10.1039/c8ay00677f

‡ Zhengwei Xiong and Haixia Zhong contributed equally to this work.

H–rGO can precipitate in high concentrations of salt solution. The BPA aptamer can adsorb on the surface of H–rGO to protect them against salt-induced aggregation. Therefore, the corresponding supernatant contains more dispersed H–rGO and shows deep blue color after the chromogenic reaction. However, in the presence of BPA, the aptamer can specifically bind to BPA; this results in the escape of the aptamer from the H–rGO surface and the salt-induced aggregation of H–rGO. The corresponding supernatant contains a little H–rGO and shows light blue color after the chromogenic reaction. The color difference can be used for the quantitative detection of BPA. Importantly, this method provides an easy and visible result readout platform for BPA detection.

2. Experimental

2.1 Reagents and apparatus

Graphene oxide (GO) was purchased from Tanyuan Graphene Co., Ltd (China). Hemin was obtained from Bomei Biotechnology Co., Ltd (China). Hydrazine hydrate (85%), 3,3′,5,5′-tetramethylbenzidine (TMB), and H_2O_2 (30%) were purchased from ChengDu Chron Chemicals Co., Ltd (China). The BPA aptamer sequence (5′-CCG GTG GGT GGT CAG GTG GGA TAG CGT TCC GCG TAT GGC CCA GCG CAT CAC GGG TTC GCA CCA-3′) was synthesized by Sangon Biotech Co., Ltd (China). Tris–HCl buffer solution was purchased from Phygene Life Sciences Co., Ltd (China). Ultrapure water with a resistivity of 18.2 MΩ cm was used throughout the study.

The UV-vis absorption spectra were obtained using the Shimadzu UV-1800 spectrophotometer (Japan) with a 10 mm path length cuvette at room temperature. The UV-vis spectra were obtained from 500 to 800 nm, and the Δ absorbance intensity (the difference of absorbance at 652 nm and 757 nm) was used for BPA concentration quantitation.

SPA300-HV atomic force microscopy (AFM) (Seiko, Japan) was used to characterize the morphology of H–rGO.

2.2 Synthesis of H–rGO

The H–rGO composites were synthesized according to a ref. 24. Typically, 10 mg of GO was added to 20 mL of water and sonicated for 1 h to obtain a homogeneous dispersion. The 20 mL as-prepared GO dispersion was mixed with 20 mL of 0.5 mg mL^{-1} hemin solution and shaken for several minutes; then, 200 μL ammonia solution and 30 μL hydrazine hydrate were added in sequence and stirred for 1 h. After this, the solution was heated to 60 °C under vigorous stirring for another 3.5 h. The dispersion was then rinsed several times and centrifuged for 30 min. The H–rGO was redispersed in water for further use.

2.3 Colorimetric detection of BPA

Briefly, 40 μL BPA sample was mixed with 40 μL of 50 nM aptamer solution and then incubated for 30 min. Following this, 80 μL of H–rGO solution (0.3 mg mL^{-1}) was added to the abovementioned solution followed by vigorous shaking. Then, NaCl was added to the solution with a final concentration of 0.1 M. After 10 min incubation, the solution was centrifuged for 8 min, and the speed of centrifugation was 6000 rpm. Finally, 30 μL of the supernatant was added to 790 μL of solution containing 0.6 mM TMB and 10 mM H_2O_2 for the chromogenic reaction.

3. Results and discussion

3.1 Principle of the detection of BPA

The principle of the proposed strategy for the detection of BPA is shown in Scheme 1. H–rGO can deeply aggregate in high concentrations of salt solution.[38] Aptamer can be adsorbed on the surface of H–rGO by the π–π stacking interactions, preventing H–rGO from the salt-induced aggregation. Therefore, the supernatant with high amount of H–rGO can catalyze the oxidation of TMB to exhibit deep blue color with high absorbance intensity. However, in the presence of BPA, the aptamer can bind with its target due to strong affinity interaction; this results in the escape of the aptamer from the H–rGO surface and then the aggregation of H–rGO. Consequently, the supernatant of the solution contains very little H–rGO, showing light blue color and low absorption intensity. Thus, the color difference can be used for the quantitative detection of BPA.

3.2 Characterization of the H–rGO composites

The UV-vis absorption spectrum of the synthesized H–rGO was monitored. As shown in Fig. 1A, GO has a maximum absorption peak at 230 nm, which is derived from the π–π* transition of aromatic C=C, and a shoulder at 290–300 nm, which corresponds to the n–π* transition of the C=O bond.[39] Hemin has two special feature absorptions: a strong peak at 386 nm for the Soret absorption band (the B absorption band) and a group of weak peaks between 480 and 670 nm for the Q-absorption band.[24] Moreover, H–rGO has two absorption peaks at 265 nm and 418 nm. The broad absorption peak at 265 nm corresponds to GO with a red shift of 35 nm, and the absorption peak at 418 nm corresponds to the Soret absorption band of hemin with a red shift of 32 nm.[40] The red shift represents the mutual interaction effect between graphene and hemin. The surface of the H–rGO nanosheet was characterized by AFM (Fig. 1B). The average thickness of the H–rGO nanosheet was about 1.2 nm (Fig. 1B). There was about 0.25 nm increment as compared to the case of GO (Fig. S1†). This can be attributed to the single layer of hemin (0.2 nm) absorbed on the GO surface.[41] These results indicated that H–rGO was successfully synthesized.

3.3 Feasibility investigation of the proposed strategy

We designed experiments to investigate the feasibility of this strategy. The absorption spectra and color of the samples under different conditions were studied (Fig. 2A and B). The Δ absorbance (the difference of absorbance at 652 nm and 757 nm) was used to evaluate the color degree of the chromogenic reaction. As shown in Fig. 2A, the Δ absorbance intensity of sample 1 without H–rGO was near 0, indicating that the chromogenic reaction could not be carried out in the absence of hemin. Sample 2 with GO and sample 3 with rGO also show

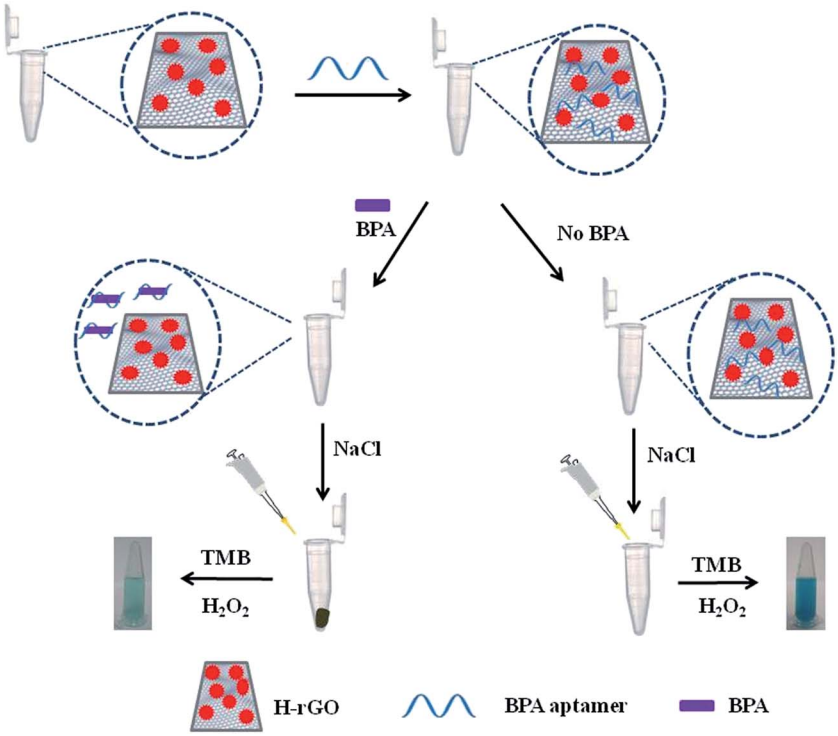

Scheme 1 Schematic of the design strategy for BPA based on peroxidase-like activity of H–rGO and aptamer.

similar Δ absorbance intensity due to the same reason. However, the aptamer can be strongly adsorbed on the rGO surface by the π–π stacking interactions, preventing the H–rGO from aggregation. More H–rGO in the supernatant can result in a high Δ absorbance intensity and darker blue color (sample 4). The Δ absorbance intensity of sample 5 without aptamer is much lower than that of sample 4. This can be attributed to the aggregation of H–rGO in salt solution without aptamer protection, and a light blue color is exhibited. We have noticed that the Δ absorbance of sample 6 is also relatively low; this is because the aptamer can bind with its target (BPA) due to its strong affinity interaction with BPA, and the aggregations of H–rGO and light blue color are observed. The high Δ absorbance intensity of sample 7 is similar to that of sample 3; this indicates that a random sequence cannot bind with BPA; this results in good dispersion status of H–rGO and dark blue color. All the results are in accordance with our expectations and detection principles.

3.4 Optimization of detection conditions

Experimental conditions have significant influence on the performance of this strategy. We optimized some key parameters including pH of the incubation solution and concentrations of TMB, H_2O_2 and NaCl. Because the catalytic activity of H–rGO was highly affected by the pH of solution, the pH of the

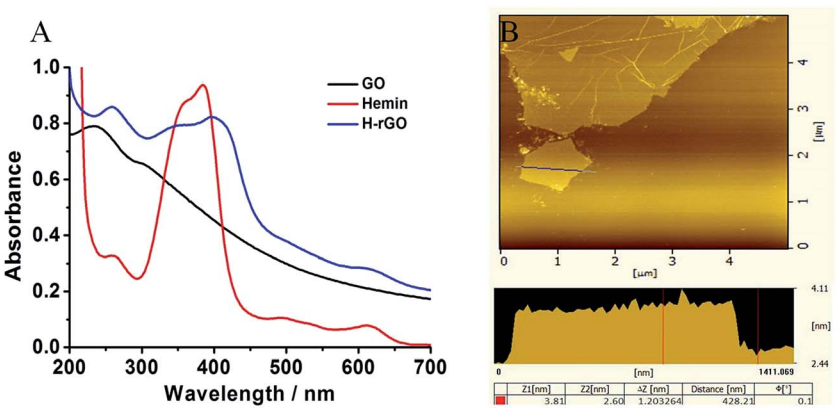

Fig. 1 (A) UV-visible absorption spectra of GO, hemin and H–rGO suspension and (B) AFM characterization of H–rGO sheets on mica substrate and the cross section identified by the line shows the heights of H–rGO.

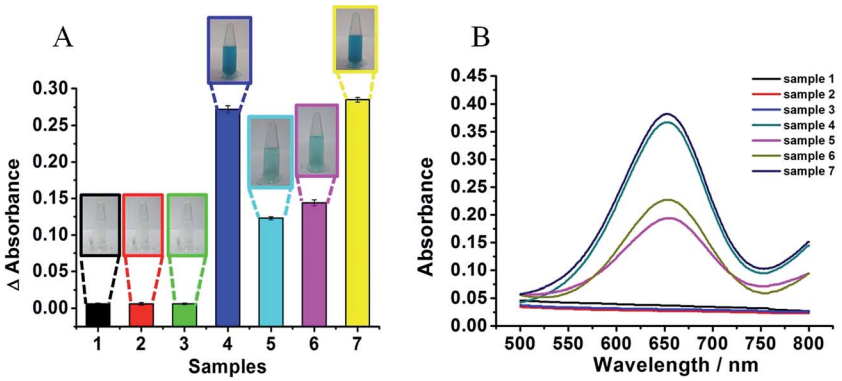

Fig. 2 The Δ absorbance intensity (A) and UV-vis absorption spectra (B) of H–rGO solution under different conditions: (1) 50 nM aptamer and 85 nM BPA without H–rGO in 0.1 M NaCl, (2) 50 nM aptamer and 85 nM BPA with GO in 0.1 M NaCl, (3) 50 nM aptamer and 85 nM BPA with rGO in 0.1 M NaCl, (4) H–rGO and 50 nM aptamer without BPA in 0.1 M NaCl, (5) H–rGO and 85 nM BPA without aptamer in 0.1 M NaCl, (6) H–rGO, 50 nM aptamer and 85 nM BPA in 0.1 M NaCl, and (7) H–rGO, 50 nM random sequence and 85 nM BPA in 0.1 M NaCl.

reaction solution was related to the catalytic ability of hemin on H–rGO. As shown in Fig. 3A, the Δ absorbance intensity of the solution increases with the pH value and then drops sharply when the pH is over 5. This can be because weakly acidic solutions can enhance the catalytic oxidizability of H–rGO to TMB, causing distinguished deep blue color after the chromogenic reaction. However, the hemin on H–rGO can be denatured under strong acidic or alkaline conditions; this results in a distinguished light blue color after the chromogenic reaction. Therefore, an incubation solution with pH 5 was used in our experiments.

The concentration of H_2O_2 has a significant influence on the catalytic oxidation process; the concentration of H_2O_2 has been tuned from 0 to 20 mM. This result could be seen from Fig. 3B; the Δ absorbance intensity of the solution increased with H_2O_2 concentrations and reached a plateau around 10 mM. Therefore, 10 mM of H_2O_2 was chosen for the chromogenic reaction.

The effect of TMB concentration on the chromogenic reaction is shown in Fig. 3C; the concentration of TMB has been tuned from 0 to 1000 μM. The Δ absorbance intensity of the reaction system increases with TMB concentrations and is stale around 600 μM. Thus, 600 μM of TMB was used for the chromogenic reaction.

The concentration of sodium chloride affects the degree of agglomeration of H–rGO.[32] The effect of different salt concentrations on the Δ absorbance intensity is shown in Fig. 3D.

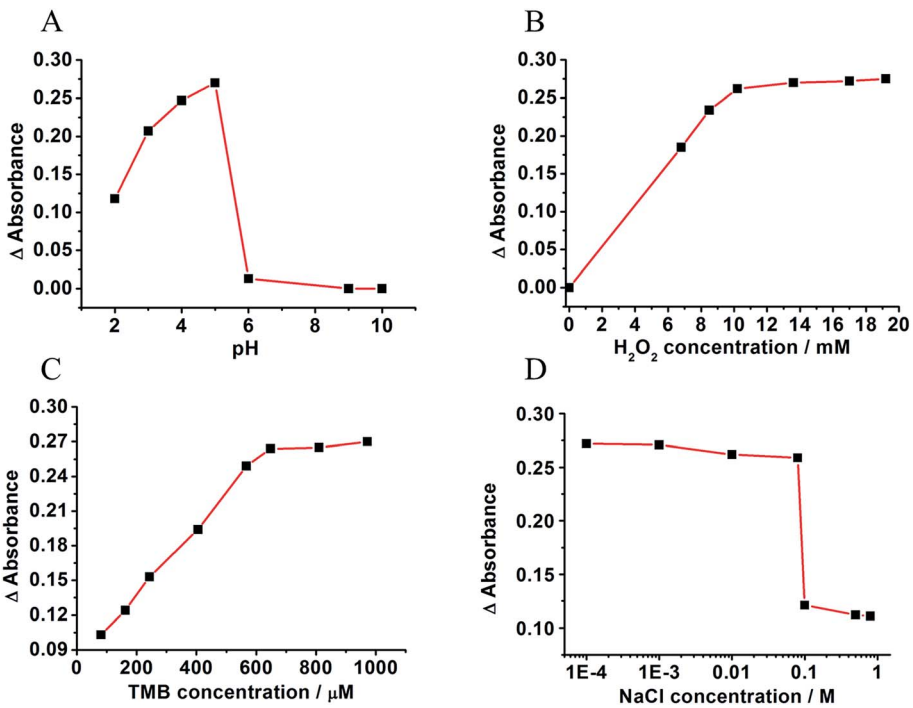

Fig. 3 The influence of different values of pH (A) and concentration of H_2O_2 (B), TMB (C), and NaCl (D) on the Δ absorbance intensity.

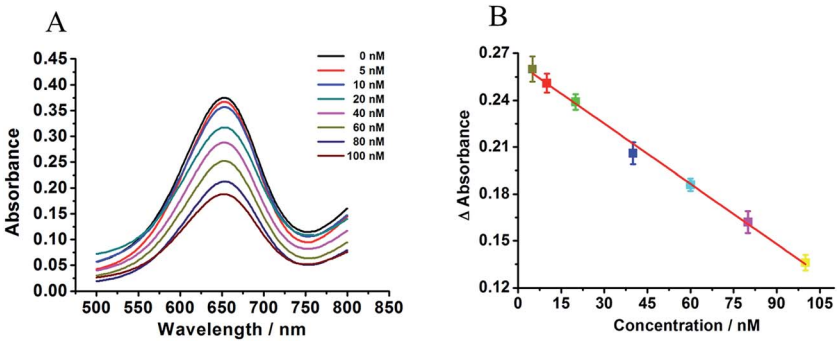

Fig. 4 (A) UV-vis spectra for different concentrations of BPA (5 nM, 10 nM, 20 nM, 40 nM, 60 nM, 80 nM and 100 nM). (B) The calibration curve for BPA sensing from 5 nM to 100 nM.

When the salt concentration is too low, the Δ absorbance intensity is stable; this indicates that the aggregation of H–rGO is hardly induced. However, H–rGO aggregates heavily when the concentration of NaCl is over 0.1 M; this results in significant decrease of the Δ absorbance intensity. Therefore, the salt concentration of 0.1 M was chosen for this experiment.

3.5 Analytical performance for BPA detection

The sensitivity and linearity were evaluated under the best experimental conditions. As shown in Fig. 4A, the Δ absorbance intensity decreases gradually with an increase in the BPA concentration from 5 nM to 100 nM. The Δ absorbance intensity and BPA concentration show a good linear correlation in the range from 5 to 100 nM, and the correlation coefficient (R^2) is 0.997. The detection limit is 2 nM, which is calculated by three times the standard deviation of the blank. The sensitivity of this method is comparable to that of other reported BPA aptamer sensors (Table S1†). In addition, the label-free condition and visible result readout platform offer significant advantages for rapid and portable applications.

3.6 Evaluation of the selectivity of this method

The absorption intensity of different analogs, including bisphenol B (BPB), bisphenol C (BPC), bisphenol A ethoxylate (BPE), bisphenol F (BPF), diethylstilbestrol (DES), 17β-estradiol (E2), and estriol (E3) (chemical structures shown in Fig. S2†) was used to evaluate the selectivity of the sensing method. The results show that only the BPA sample can result in weak Δ absorbance intensity, proving the aggregation of H–rGO. The influence of other analogs can almost be neglected. It showed the excellent selectivity of this method for BPA detection. The good selectivity can be attributed to the high affinity interaction between the aptamer and BPA (Fig. 5).

3.7 Real sample detection

The practical applications of this method were studied using tap water samples. The tap water samples were first filtered with a 0.45 μm membrane, and then, the pH of the sample was adjusted to 5 before detection. Herein, three different concentrations (15, 50 and 100 nM) of BPA were spiked in tap water. As shown in Table 1, the recoveries changed from 88.55% to 97.06%, and the RSDs ranged from 6.35% to 10.61%. These results indicated that the performance of this method satisfied the requirement for real applications.

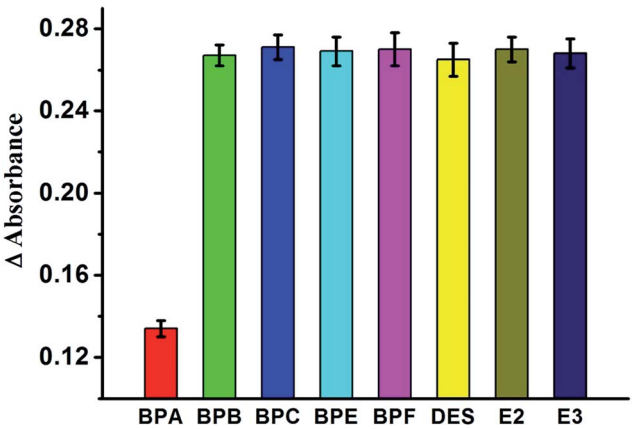

Fig. 5 Selectivity of the proposed method for BPA detection over other analogs. The concentrations are 100 nM for BPA and 1 μM for other analogs.

Table 1 Determination of BPA in tap water *via* the proposed method[a]

Sample	Spiked/nM	Found/nM	Recovery/%	RSD/% (six replicates)
Tap water 1	0	ND	ND	ND
Tap water 2	15.00	14.56	97.07	7.68
Tap water 3	50.00	45.89	91.78	10.61
Tap water 4	100.00	88.55	88.55	6.35

[a] "ND": not detected.

4. Conclusions

In summary, a fast and visible strategy has been developed for BPA detection based on H–rGO and aptamer. This strategy takes advantages of the aggregation ability of H–rGO at high salt concentrations and protecting ability of aptamer from salt induced H–rGO precipitation. The proposed method exhibits

a good linear range from 5 to 100 nM with a low detection limit of 2 nM. It has been successfully used for real sample detection. In addition, the label-free condition and visible result readout platform offer significant advantages for rapid and portable applications.

Conflicts of interest

There are no conflicts to declare.

Acknowledgements

This work was sponsored by the Project of Wenzhou Science &Technology Bureau (W20170006, S20150012), the Opening Project of Zhejiang Provincial Top Key Discipline of Pharmaceutical Sciences (Grant No. 201712), the Science and Technology Research Program of Chongqing Municipal Education Commission (Grant No. KJ1601404, KJ1706156), the Open Project of State Key Laboratory Cultivation Base for Nonmetal Composites and Functional Materials (Grant No. 17kffk06), the Scientific Research Program of Chongqing University of Education (Grant No. KY201550C), and the Program of Innovation Center of Lipid Resources and Children's Daily Chemicals at Chongqing University of Education (Grant No. 2017XJPT01).

References

1 J. Chen and S. Zhou, *Biosens. Bioelectron.*, 2016, **77**, 277–283.
2 K. Deng, X. Liu, C. Li, Z. Hou and H. Huang, *Anal. Methods*, 2017, **9**, 5509–5517.
3 J. T. Wolstenholme, E. F. Rissman and J. J. Connelly, *Horm. Behav.*, 2011, **59**, 296–305.
4 J. R. Rochester, *Reprod. Toxicol.*, 2013, **42**, 132.
5 F. Sun, L. Kang, X. Xiang, H. Li, X. Luo, R. Luo, C. Lu and X. Peng, *Anal. Bioanal. Chem.*, 2016, **408**, 1–15.
6 G. Gao, H. Chen, L. Zhu, Y. Chai, G. Ma, C. Wang, Z. Hao, X. Liu and C. Lu, *Anal. Methods*, 2017, **9**, 6769–6776.
7 K. V. Ragavan, N. K. Rastogi and M. S. Thakur, *Trends Anal. Chem.*, 2013, **52**, 248–260.
8 N. K. Temel and R. Gürkan, *Anal. Methods*, 2017, **9**, 1190–1200.
9 N. Kuroda, Y. Kinoshita, Y. Sun, M. Wada, N. Kishikawa, K. Nakashima, T. Makino and H. Nakazawa, *J. Pharm. Biomed. Anal.*, 2003, **30**, 1743–1749.
10 Y. Yoon, P. Westerhoff, S. A. Snyder and M. Esparza, *Water Res.*, 2003, **37**, 3530–3537.
11 A. C. Dirtu, L. Roosens, T. Geens, A. Gheorghe, H. Neels and A. Covaci, *Anal. Bioanal. Chem.*, 2008, **391**, 1175–1181.
12 H. Flood and W. J. Knapp, *Toxicol. Mech. Methods*, 2006, **16**, 427–430.
13 T. Tominaga, T. Negishi, H. Hirooka, A. Miyachi, A. Inoue, I. Hayasaka and Y. Yoshikawa, *Toxicology*, 2006, **226**, 208–217.
14 M. A. M. Fernandez, L. C. André and Z. de Lourdes Cardeal, *J. Chromatogr. A*, 2017, **1481**, 31–36.
15 S. h. Chung and W. h. Ding, *J. Pharm. Biomed. Anal.*, 2018, **149**, 572–576.
16 J. Kawakami, H. Imanaka, Y. Yokota and N. Sugimoto, *J. Inorg. Biochem.*, 2000, **82**, 197–206.
17 J. Liu, Z. Cao and Y. Lu, *Chem. Rev.*, 2009, **109**, 1948–1998.
18 X. Zuo, S. Song, J. Zhang, D. Pan, A. L. Wang and C. Fan, *J. Am. Chem. Soc.*, 2007, **129**, 1042.
19 A. Y. Lee, N. R. Ha, I. P. Jung, S. H. Kim, A.-R. Kim and M.-Y. Yoon, *Anal. Biochem.*, 2017, **531**, 1–7.
20 G. S. Bang, S. Cho, N. Lee, B. R. Lee, J. H. Kim and B. G. Kim, *Biosens. Bioelectron.*, 2013, **39**, 44–50.
21 H. Shu, H. Mei, J. Gu, Y. Yang, B. Chen, L. Huang, Q. Wang, X. Chen, D. Li and J. Gao, *Anal. Methods*, 2017, **9**, 5115–5120.
22 X. Yang, J. Qian, L. Jiang, Y. Yan, K. Wang, Q. Liu and K. Wang, *Bioelectrochemistry*, 2014, **96**, 7–13.
23 L. Zhou, H. Cheng, J. E. Wang and R. J. Pei, *Chin. J. Anal. Chem.*, 2016, **44**, 13–18.
24 Y. Guo, L. Deng, J. Li, S. Guo, E. Wang and S. Dong, *ACS Nano*, 2011, **5**, 1282–1290.
25 T. Xue, S. Jiang, Y. Qu, Q. Su, R. Cheng, S. Dubin, C. Y. Chiu, R. Kaner, Y. Huang and X. Duan, *Angew. Chem.*, 2012, **51**, 3822.
26 W. Wei, D. M. Zhang, L. H. Yin, Y. P. Pu and S. Q. Liu, *Spectrochim. Acta, Part A*, 2013, **106**, 163–169.
27 L. Gao, J. Zhuang, L. Nie, J. Zhang, Y. Zhang, N. Gu, T. Wang, J. Feng, D. Yang and S. Perrett, *Nat. Nanotechnol.*, 2007, **2**, 577.
28 Y. J. Long, Y. F. Li, Y. Liu, J. J. Zheng, J. Tang and C. Z. Huang, *Chem. Commun.*, 2011, **47**, 11939–11941.
29 Y. Song, K. Qu, C. Zhao, J. Ren and X. Qu, *Adv. Mater.*, 2010, **22**, 2206–2210.
30 T. Lin, L. Zhong, J. Wang, L. Guo, H. Wu, Q. Guo, F. Fu and G. Chen, *Biosens. Bioelectron.*, 2014, **59**, 89.
31 T. Lin, L. Zhong, L. Guo, F. Fu and G. Chen, *Nanoscale*, 2014, **6**, 11856.
32 T. Lin, L. Zhong, Z. Song, L. Guo, H. Wu, Q. Guo, Y. Chen, F. F. Fu and G. Chen, *Biosens. Bioelectron.*, 2014, **62**, 302–307.
33 L. Ai, L. Li, C. Zhang, J. Fu and J. Jiang, *Chem.–Eur. J.*, 2013, **19**, 15105–15108.
34 X. Xu, M. Wei, Y. Liu, X. Liu, W. Wei, Y. Zhang and S. Liu, *Biosens. Bioelectron.*, 2017, **87**, 600–606.
35 Y. Guo, J. Li and S. Dong, *Sens. Actuators, B*, 2011, **160**, 295–300.
36 W. Wei, D. Zhang, H. Li, L. Yin, Y. Pu and S. Liu, *Microchim. Acta*, 2014, **181**, 1557–1563.
37 H. Wei and E. Wang, *Chem. Soc. Rev.*, 2013, **42**, 6060–6093.
38 Z. Yang, J. Qian, X. Yang, D. Jiang, X. Du, K. Wang, H. Mao and K. Wang, *Biosens. Bioelectron.*, 2015, **65**, 39–46.
39 R. Oprea, S. F. Peteu, P. Subramanian, W. Qi, E. Pichonat, H. Happy, M. Bayachou, R. Boukherroub and S. Szunerits, *Analyst*, 2013, **138**, 4345–4352.
40 H. Song, Y. Ni and S. Kokot, *Anal. Chim. Acta*, 2013, **788**, 24–31.
41 Y. Qutub, V. Uzunova, O. Galkin and P. G. Vekilov, *J. Phys. Chem. B*, 2010, **114**, 4529–4535.